Multiscale simulation of dilute DNA in a roll-knife coating flow

Rajat Duggal[a)]

Department of Chemical and Biomolecular Engineering, Rice University, MS362, 6100 Main Street, Houston, Texas 77005

P. Sunthar[b)] and J. Ravi Prakash[c)]

Department of Chemical Engineering, Monash University, Melbourne, Victoria 3800, Australia

Matteo Pasquali[c)]

Department of Chemical and Biomolecular Engineering, Rice University, MS362, 6100 Main Street, Houston, Texas 77005

(Received 21 April 2008; final revision received 15 September 2008)

Synopsis

The dynamics of dilute solutions of DNA flowing in a scaled down roll-knife coating flow are investigated on multiple scales. The flow is generated between a rotating roll and a stationary glass knife, and extension of fluorescently stained DNA molecules is measured at the minimum gap at low roll speeds. The macroscopic flow is computed by solving the continuum equations of motion with the finite element method; the microscale behavior of DNA molecules is predicted by Brownian dynamics combined with successive fine-graining. The simulations predict that the DNA should stretch almost to full extension near the roll surface in the region of minimum gap; this does not agree with experimental measurements. The assumption that the flow is nearly homogeneous on the length scale of the polymer molecules, commonly used in processing flows as well as Brownian dynamics simulations of simple flows, fails near free surfaces, and is the likely cause of the discrepancy. Evidence from the literature suggests that similar nonlocal effects may be present in coating and ink-jet printing flows of high molecular weight polymer solutions. © *2008 The Society of Rheology.* [DOI: 10.1122/1.2994729]

I. INTRODUCTION

Understanding the interplay of flow and polymer microstructure in complex flows is key for designing and controlling important processes such as ink-jet printing, spraying, and coating. Coating operations are an essential part of manufacturing processes for

[a)]Present address: The Dow Chemical Company, 2301 N. Brazosport Blvd., Freeport, TX 77541.
[b)]Present address: Dept. of Chemical Engineering, Indian Institute of Technology, Bombay, Mumbai, Powai-400 076 Maharashtra, India.
[c)]Authors to whom correspondence should be addressed; electronic mail: ravi.jagadeeshan@eng.monash.edu.au and mp@rice.edu

commodity and specialty products—painted metal in automobiles and appliances, photographic films, coatings for memory storage in video tapes and diskettes, coatings of substrates to make biosensors and DNA chips, and novel methods for manufacturing photonic crystals. Coating liquids are complex fluids because they consist of a combination of polymers, surfactant, and nano- and microparticles dissolved or suspended in a low-molecular weight liquid. In 2003, coated products and coating processes contributed about $18 billion to the US economy [Tullo (2004)]. Thus, the interaction of flow and microstructure in coating processes is a very important problem both at the fundamental as well as the applied level. The present study focuses on roll-knife coating, one of the workhorses of coating technology.

In complex fluids the flow and the configuration (conformation) of the microstructure are coupled. Together with imposed boundary conditions, the interplay between the two determines the flow pattern and its stability. The velocity convects the microstructure in the liquid, while the velocity gradients act to deform the microstructure which induces stress in the microstructure. When the stress due to the microstructure is comparable or larger than pressure and viscous stress, the flow field changes, sometimes dramatically. For example, the addition of small amount of polymer in a liquid can suppress droplet breakup in spraying, which is desirable [Marano *et al.* (1997)]; in roll coating, polymer molecules can enhance ribbing which causes nonuniformity in the coated product [Dontula (1999)], which is undesirable. The equations governing free surface flows of complex fluids are nonlinear (and still poorly defined in certain cases); therefore, analytical solutions cannot be obtained. Thus, computer simulations are required to understand this interplay of the flow and the fluid microstructure. Molecular models describing polymer microstructure have been developed and validated against experiments in simple flows [Hur *et al.* (2002, 2001, 2000); Jendrejack *et al.* (2002); Sunthar and Prakash (2005)]. However, the development of system-level simulations that can capture the behavior of the materials in complex inhomogeneous flows is still in its infancy. Recent advances in measurement of microscopic quantities using single molecule visualization of DNA [Perkins *et al.* (1997); Smith *et al.* (1999)] have made it possible to study the effect of the flow on polymer microstructure and have aided development and validation of simulation schemes in simple shear and extension flows. Understanding molecular behavior in more complex inhomogeneous flows of relevance is clearly the next challenge.

The stretch and orientation of DNA molecules in a roll-knife coating flow was recently measured using single molecule visualization [Duggal and Pasquali (2004)]. Here, the macroscopic two-dimensional roll-knife coating flow field is computed and the conformation of individual DNA molecules is simulated along streamlines and compared to the previously reported measurements.

A. Background

The most common coarse-grained molecular models represent polymer chains as a sequence of beads connected with rods (bead-rod model) or beads connected with springs (bead-spring model) [Bird *et al.* (1987)]. In the bead-rod model for flexible polymers, the beads are connected in series by rigid rods of length equal to the Kuhn length—the characteristic step size of a random walk [Flory (1953)]. Only the beads experience frictional drag from the solvent and the flow does not affect the configuration of the chain at scales below the Kuhn length. Bead-rod models are computationally expensive because the number of beads becomes large with increasing molecular weight (increasing the number of variables). For example, a typical λ-DNA molecule has about 200 Kuhn steps, and a 1.95 Mg/mol polystyrene (PS) molecule has 2627 Kuhn steps [Prabhakar *et al.*

(2004)]. These numbers exceed the current capabilities for extensive simulation studies of such polymer molecules (about 100 Kuhn steps). Instead, in a bead-spring model many Kuhn lengths are grouped together and replaced by a spring with an appropriate force law; with increasing molecular weight, the effective spring constant of the connector springs can be suitably modified to model larger groups of Kuhn steps without increasing the number of beads.

To describe the nonequilibrium behavior of dilute solutions of flexible polymers using the coarse-grained molecular theories, it is essential to consider the various forces and interactions that determine molecular conformations in flows. Solvent molecules continuously collide with polymer segments, imparting random (fluctuating) Brownian forces. The flowing solvent exerts a frictional drag force on the chain because of momentum exchange due to the (average) velocity difference between a portion of the chain and the surrounding solvent [Bird *et al.* (1987)]. The motion of a part of the polymer chain alters the velocity field and induces additional forces on the rest of the chain—these forces are termed "hydrodynamic interactions" [Larson (1999)]. Other important intramolecular interaction forces arise from "excluded volume interactions." Excluded volume (EV) effects become important in flexible polymers when monomer segments, though distant along a chain, interact to repel each other as they come close to each other in space. This interaction, which is absent in ideal chains obeying Gaussian statistics (or at θ conditions), leads to a swelling of the polymer size [Doi and Edwards (1986)], and modifies both equilibrium and rheological properties. In the case of DNA solutions, the charged backbone of the DNA leads to long range interactions and as a result the molecule is normally not flexible; however, in the presence of excess salt the electrostatic repulsion is screened [Barrat and Joanny (1996)] leading to an effective short-ranged repulsion. The DNA chain is then expected to behave like a neutral polymer in a good solvent. To obtain quantitative agreement of the behavior of DNA molecules under flow, therefore, EV interactions need to be incorporated.

Until recently, the predictions of statistical theories of polymer solution dynamics [Flory (1953); Rouse (1953); Zimm (1956)] could be compared with only bulk rheological and optical measurements. Direct video microscopy of individual DNA molecules provided the first direct measurement of the behavior of individual molecules—see, e.g., Shaqfeh (2005) for a recent review. The success of the single molecule visualization technique in studying simple homogeneous shear [Smith and Chu (1998)], elongational [Perkins *et al.* (1995)], and mixed [Babcock *et al.* (2003)] flows has paved the way for studying more complex and relevant inhomogeneous flows. The molecular properties of DNA in simple homogeneous flows have been studied computationally using the bead-rod and bead-spring molecular models. Larson *et al.* (1999) used the bead-spring model with the worm-like chain spring force [Marko and Siggia (1995)], taking into account only the Brownian force and the drag force to describe the dynamics of DNA molecules subjected to a planar extensional flow. The quantitative predictions of the ensemble average stretch and rate of stretch from the Brownian dynamics simulations agreed with the single molecule DNA experiments performed by Perkins *et al.* (1997) and Smith and Chu (1998). Molecular individualism, i.e., dependence on initial configuration [de Gennes (1997); Perkins *et al.* (1997)], observed in the experiments was also captured by the simulations, and various molecular configurations such as folds, kinks, dumbbells and half-dumbbells were predicted by the coarse-grained model. Hur *et al.* (2000) performed Brownian dynamics of bead-rod and bead-spring (finitely extensible nonlinear elastic spring, i.e., FENE, or worm-like) chains to study molecular behavior in pure shear flow. The models captured the stretch-tumble dynamics observed in the experiments and the measured average extension of DNA molecules [Smith *et al.* (1999)] was accurately

predicted by the simulations. These simulations were extended to study the transient response of molecular extension in start-up shear flows by Babcock *et al.* (2000). Hur *et al.* (2001) combined fluorescence microscopy, bulk rheological measurements, and Brownian dynamics to understand the coupling of the flow with the DNA microstructure in dilute and semidilute solutions. They found no effect of concentration (ultradilute to six times the overlap concentration) on the individual dynamics of the DNA molecules. In all these simulations the chains deformed under the action of only Brownian and drag forces. Jendrejack *et al.* (2002) also used a bead-spring chain model with a worm-like chain spring force and predicted the DNA extension in shear flows; they also incorporated excluded volume and hydrodynamic interactions in the simulations. Dynamics of single DNA molecules were also studied in homogeneous linear mixed flows using Brownian dynamics by Hur *et al.* (2002). They predicted that when the strain rate exceeds the vorticity (extension dominated flows) the molecules deform to almost fully stretched state and when the vorticity exceeds the strain rate (rotation dominated flows) the molecules deform in a periodic motion with an average extension lower than that observed in simple shear flows. These predictions were confirmed experimentally by Babcock *et al.* (2003).

More recently, single molecule DNA visualization has complemented Brownian dynamics simulation in studying complex flows generated in drying drops of DNA solutions [Chopra *et al.* (2003)]. The stretch and orientation of DNA on substrates were predicted by using a convection flow computed from lubrication approximation. Wall hydrodynamics were neglected in these simulations. However, these are important because the molecules flow very close to the substrate and adsorb on the surface; thus, the study, though significant, is controversial. Jendrejack *et al.* (2003) extended the Brownian dynamics simulation method to incorporate long-range hydrodynamic interactions with walls in a confined geometry. They studied the dynamics of long DNA molecules (up to 100 μm) in a pressure-driven flow in rectangular microchannels and found that wall hydrodynamics cause a depletion in the concentration of DNA near the wall due to cross-stream migration. This discovery was confirmed experimentally by Fang *et al.* (2005), who found a depletion layer of 7 μm next to the walls.

In all the aforementioned computational studies on DNA dynamics in flows the model parameters were obtained by fits to experimental data, either all measured at equilibrium or a combination of equilibrium and flow measurements. Sunthar and Prakash (2005) and Sunthar *et al.* (2005) used Brownian dynamics simulations to model DNA in elongational flow using a rescaling approach where parameter-free predictions of the molecular properties were obtained. The DNA molecule was represented by a finitely extensible bead-spring model, and excluded-volume and hydrodynamic interactions between the beads were taken into account. A successive fine graining of the polymer chain was performed by progressively increasing the number of beads, and predictions of the microscopic extension were computed in the limit of large number of beads, where they became insensitive to both chain discretization and the initial choice of the parameters used for hydrodynamic and excluded-volume interactions. The theoretical predictions compared well with the experimental observations of DNA stretch by Smith and Chu (1998), and extensional stresses in DNA solutions measured with the filament stretching rheometer [Sunthar *et al.* (2005)]. In this study we tested the parameter free rescaling approach in a relevant complex coating flow using a multiscale method.

II. MULTISCALE METHOD

The multiscale method presented here to study the interplay of flow and polymer microstructure combines single molecule measurements in the flow of interest [Duggal

and Pasquali (2004)] with simulation of the polymer microstructure in the computed macroscopic flow field. The flow was generated in a roll-knife coating flowcell [Duggal and Pasquali (2004)] which had been scaled down to fit under a microscope, while keeping relevant length (i.e., coating gap) and time (i.e., shear rate) scales in the typical range of actual coating flows. The evolution of DNA microstructure was investigated in ultradilute polymer solutions where the polymer molecules behave as if they were in dilute solutions; however, because the concentration of polymer molecules is so incredibly low, the fluid behaves essentially as Newtonian [Duggal and Pasquali (2004); Harrison *et al.* (1998); Pasquali (2000)]. This allows the separation of the effect of flow on the polymer microstructure from the converse effect of the polymer microstructure on the flow. Essentially, DNA was used as a "macromolecular tracer" in a Newtonian flow field—the liquid in the microscopy experiment was a Newtonian sugar solution. The molecular conformation was observed and measured using single molecule fluorescence microscopy.

The flow was computed by solving the Navier–Stokes equations with the Galerkin/finite element method and compared with experimental measurements. DNA was modeled as a chain of beads connected with springs; the evolution of the DNA in the flow was computed, and compared with experimental measurements, as described below.

A. Continuum flow calculation

The two-dimensional Newtonian free surface flow in the roll-knife coating flowcell was computed using the method and software developed by Carvalho [Carvalho (1996); Carvalho and Kheshgi (2000)] and Pasquali [Pasquali (2000); Pasquali and Scriven (2002)]. The method is based on mapping the unknown flow domain (physical domain) into a computational domain by using the elliptic mesh generation method [Christodoulou (1990)]. The mapping $\boldsymbol{\xi}=\boldsymbol{\xi}(\mathbf{x})$ between the computational domain $\boldsymbol{\xi}$ and the physical domain $\mathbf{x}$, obeys the elliptic differential equation

$$\nabla\cdot\tilde{\mathbf{D}}\cdot\nabla\boldsymbol{\xi}=0, \tag{1}$$

where $\nabla\equiv\partial/\partial\mathbf{x}$ denotes differentiation in physical space, and the dyadic $\tilde{\mathbf{D}}$ controls the spacing of the ξ_1 and ξ_2 coordinate lines [de Santos (1991); Pasquali (2000)]. Because of the complex geometry of the flow setup, the physical domain was divided into simpler, connected, quadrangular subdomains, each of which was then mapped onto a separate subdomain of the computational domain.

The domain boundaries were described by the geometry of the experimental flowcell [experiments E4 and E8 in Duggal and Pasquali (2004)]. The radius of the roll was $R=6.35$ mm, and the minimum gap between the top of the roll and the coverslip was $H=35.3$ μm. The roll rotated at 0.05 rps.

The transport equations of mass and momentum in a steady, isothermal, incompressible liquid are

$$0=\nabla\cdot\mathbf{v}, \tag{2}$$

$$0=\rho\mathbf{v}\cdot\nabla\mathbf{v}-\nabla\cdot\mathbf{T}-\rho\mathbf{g}, \tag{3}$$

where $\mathbf{v}$ is the liquid velocity, ρ is the liquid density, $\mathbf{T}$ is the stress tensor (Cauchy), and $\mathbf{g}$ is the gravitational acceleration. $\mathbf{T}$ is split into isotropic and viscous components, $\mathbf{T}=-p\mathbf{I}+\boldsymbol{\tau}$, where the mechanical pressure p is constitutively indeterminate because the liquid is incompressible, and the viscous stress $\boldsymbol{\tau}$ obeys Newton's law of viscosity, $\boldsymbol{\tau}=2\eta\mathbf{D}$.

The mapping was computed by solving Eq. (1) coupled with the continuity and momentum equations [Eqs. (2) and (3)] and appropriate boundary conditions using the Galerkin/finite element method. The solution (velocity, pressure, and mapping fields) was approximated in terms of simple polynomial basis functions. The differential equations were converted to a set of nonlinear algebraic equations by forming their weighted residuals (in the Galerkin method the weighting functions are the same as the basis functions) and applying boundary conditions. These were solved by Newton's method with analytical Jacobian.

At low capillary number the flow was metered and the incoming film thickness was smaller than the gap between the plate and the roll. The liquid domain in experiments extended from the coating bead into films clinging to the roll, upstream and downstream, into the cylindrical pool. For simplicity, the physical domain in the computations extended only into the film along the roll. The film thickness at the inflow and the outflow was unknown. Thus, the element nodes on the free surface at the inflow and the outflow boundary were allowed to move in the radial direction with respect to the center of the roll.

The location of the contact lines at the coverslip were also unknown. The contact lines were allowed to slide freely over the solid boundary corresponding to the coverslip. At the two contact lines the angle θ between the coordinate line ξ_i and the boundary was prescribed, $\mathbf{n}\cdot\nabla\xi_i=|\nabla\xi_i|\cos\theta$, $i=1$ or 2, where $\mathbf{n}$ is the outward pointing normal to the flow domain. The contact angle was measured independently by videomicroscopy as $\theta=35.5°$. No-penetration boundary condition $\mathbf{n}\cdot\mathbf{v}=0$ was used at the free surfaces. The position of the element nodes at the minimum gap on both the solid boundaries (roll and the coverslip) were fixed. For better mesh control the nodes were distributed on the boundary of the physical domain according to different stretching functions that controlled their spacing.

At the solid impermeable surfaces (coverslip and the roll surface) a no-slip and no-penetration condition was imposed, $\mathbf{v}=\mathbf{v}_s$ ($v_s=0$ at the coverslip and $v_s=\omega R$ at the roll). A force balance was used at the free surfaces where the shear stress exerted by the gas on the liquid was negligible and the curvature of the free surface induces a capillary pressure in the normal direction

$$\mathbf{n}\cdot\mathbf{T}=-p_a\mathbf{n}+\frac{2\mathcal{H}}{\mathrm{Ca}}\mathbf{n}, \tag{4}$$

where $\mathcal{H}$ is the mean curvature of the interface, $\mathrm{Ca}\equiv\eta V/\sigma$ is the capillary number, V is the tangential roll speed, η is the liquid viscosity, σ is the surface tension of the liquid, and p_a is the ambient pressure.

At the outflow boundary the flow was assumed to be fully developed $\mathbf{n}\cdot\nabla\mathbf{v}=0$. An appropriate boundary condition is thus required at the synthetic inflow boundary. Because the flowrate and the velocity profile at the inflow were unknown, a free boundary condition was used at the inflow boundary [Papanastasiou *et al.* (1992)]. Papanastasiou *et al.* (1992) and Carvalho (1996) found that such a boundary condition yields realistic flow states by allowing the finite-element weighted residual equation to be satisfied in a weak sense, i.e., over the interior of the boundary. All the boundary conditions are shown in Fig. 1.

Other experimental parameters were the properties of the liquid (sugar solution): viscosity $\eta=44.61$ mPa s, surface tension $\sigma=76.55$ N/m, and density $\rho=1400$ kg/m^3. Gravity was included but proved negligible.

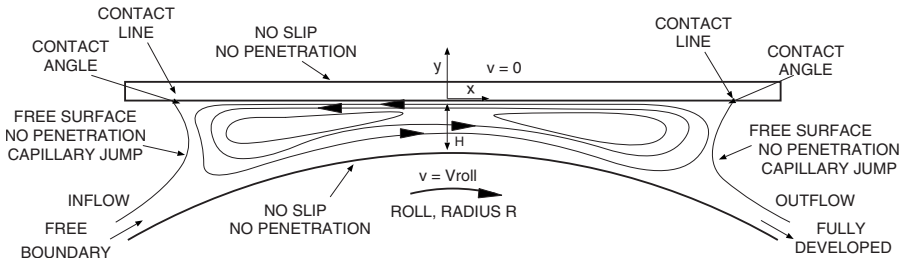

FIG. 1. Boundary conditions on the mesh, momentum, and continuity equations in the roll-knife coating flow. At the inflow a free boundary condition is used. At the outflow the flow is fully developed. No-slip and no-penetration condition was applied at the solid boundaries (roll and the coverslip). The position of the contact lines that the free surfaces make with the coverslip was not fixed, but the contact angle was fixed. A capillary force balance was used at the free surfaces.

Computing a solution required following a systematic approach, and convergence of the solution depended on the initial guess [Christodoulou *et al.* (1997)]. The coupling of the mesh and the flow was allowed sequentially. The inertialess flow was first computed on a fixed domain, i.e., the free surfaces were treated as slippery boundaries. This flow field (velocity and pressure) was used as an initial guess for solving the coupled (mapping and flow) problem upstream of the minimum gap position $x<0$; the mesh downstream $x>0$ was kept fixed. Once the upstream free surface did not change significantly the entire mesh was allowed to deform as part of the solution. The location of the inflow and outflow sections—which are artificial boundaries—was moved away from the gap repeatedly until the solution (free surface shape, film thickness, etc.) proved insensitive to further lengthening of the inflow and outflow sections.

B. Brownian dynamics

In this work a dilute solution of DNA molecules is modeled as an ensemble of noninteracting bead-spring chains, each of which has N massless spherical beads (which act as centers of hydrodynamic resistance) connected by massless springs representing an entropic force between two points on the polymer chain.

The assumptions are made that (1) the flow changes slowly on the length scale of the polymer chains, i.e., that the velocity field experienced by a chain is approximately linear and (2) that any migration of polymer molecules induced by Brownian motion or deterministic forces is negligible. Strictly, such assumptions hold only in simple homogeneous flows [Bird *et al.* (1987)]. In more complex flows, these assumptions are expected to fail in regions of rapidly varying flow, e.g., near boundaries. Nevertheless, these assumptions are almost always adopted implicitly or explicitly in processing flows—e.g., implicitly when using macroscopic equations for describing coating flows [Dimakopoulos and Tsamopoulos (2004); Lee *et al.* (2002); Pasquali and Scriven (2002)], and explicitly when using micro-macro methods in complex flows of polymeric liquids [Bajaj *et al.* (2006); Gallez *et al.* (1999); Hulsen *et al.* (1997); Laso and Öttinger (1993)]. We use these same assumptions in a roll-knife microscale flow and test their appropriateness in describing polymer dynamics in a prototypical coating flow.

The equations governing the motion of the beads is written as a set of stochastic differential equations, equivalent to a Fokker–Plank equation for the time evolution of the probability distribution function of the configuration of the bead positions [Bird *et al.* (1987); Öttinger (1996)]. The displacement of a bead position $\Delta \boldsymbol{R}$ during a finite time increment Δt^*, correct to order Δt^*, is given by [Prabhakar and Prakash (2004)],

$$\Delta \boldsymbol{R} = \left[\boldsymbol{K} \cdot \boldsymbol{R} + \frac{1}{2} \boldsymbol{D} \cdot \boldsymbol{F} \right] \Delta t^* + \boldsymbol{B} \cdot \Delta \boldsymbol{W}. \tag{5}$$

Here, $\boldsymbol{R}$ ($3N$ entries) contains the position vectors of the N beads, $\boldsymbol{K}$ contains $N \times N$ blocks of 3×3 matrices with diagonal blocks equal to $\boldsymbol{\kappa}^* \equiv \boldsymbol{\nabla} \mathbf{v}^T$ and off diagonal blocks equal to $\mathbf{0}$, $\boldsymbol{F}$ contains $3N$ components of the spring force $\mathbf{F}^{\mathrm{s}}$ and the excluded volume force $\mathbf{F}^{\mathrm{int}}$, $\boldsymbol{D}$ is the grand diffusion matrix that contains $N \times N$ blocks consisting of the elements of diffusion tensors Γ_{ij}, $\boldsymbol{W}$ is a $3N$-dimensional Wiener process, and $\mathbf{B} \cdot \boldsymbol{B}^T = \boldsymbol{D}$. In this equation, the lengths have been scaled by $l_{\mathrm{H}} = \sqrt{kT/H}$, time by $\lambda_{\mathrm{H}} = \zeta / 4H$, and forces by $\sqrt{HkT}$, where H is the Hookean spring constant, k is the Boltzmann's constant, T is the temperature, $\zeta = 6\pi\eta_{\mathrm{s}}a$ is the Stokes drag coefficient of a bead of radius a in a solvent of viscosity η_{s}.

The entropic spring force is modeled using the interpolation formula for the worm-like chain suggested for DNA [Marko and Siggia (1995)]

$$\mathbf{F}^c(\mathbf{Q}) = \mathbf{Q} \frac{1}{6q} \left[4q + \frac{1}{(1-q)^2} - 1 \right]. \tag{6}$$

where $q = Q/Q_0$ is the ratio of the magnitudes of the connector vector $\mathbf{Q}$ and the fully stretched spring length Q_0. The total spring force on the bead with index ν comes from the adjacent springs and is given by $\mathbf{F}_{\nu}^{s} = \mathbf{F}^c(\mathbf{Q}_{\nu}) - \mathbf{F}^c(\mathbf{Q}_{\nu-1})$. The EV interaction force between any two beads separated by the vector $\mathbf{r}$ is given by

$$\mathbf{F}^e(\mathbf{r}) = \frac{z^*}{d^{*5}} \exp\left(- \frac{r^2}{2d^{*2}} \right) \mathbf{r}, \tag{7}$$

where r is the magnitude of $\mathbf{r}$ and z^* and d^* are the strength and the range of the EV potential. The total EV interaction force on a bead is a sum total of the binary EV forces arising from all the other beads. Hydrodynamic interaction between two beads μ and ν were accounted for by using hydrodynamic interaction tensors $\boldsymbol{\Omega}_{\mu\nu}$ [with the Rotne–Prager–Yamakawa expression, see Öttinger (1996)]; this yields a diffusion tensor $\Gamma_{\mu\nu} = \delta_{\mu\nu}\boldsymbol{\delta} + \Omega_{\mu\nu}$. The DNA molecule was described by successive fine graining [Duggal (2006); Sunthar and Prakash (2005)] the bead-spring chain with $N = 7$, 11, 19, and 27 beads; the discretization independent conformation of the DNA chains were obtained by extrapolation to $N_k \to 250$. (See supplementary material in EPAPS document E-JORHD2-52-007806. Information on accessing this document is contained at the end of the paper.)

C. Streamline tracking

Within the Brownian dynamics algorithm, the velocity was assumed to be linear across the dimensions of the chain. The complex roll-knife coating flow is inhomogeneous, i.e., $\boldsymbol{\kappa}$ is different at each position. The algorithm used by Sunthar and Prakash (2005) was suitably modified such that in a Lagrangian frame of reference (i.e., a frame moving with the fluid velocity) $\boldsymbol{\kappa}$ was time dependent. The tracer (DNA center of mass) was constrained to move along a coarse streamline (in the fine mesh) passing through the point of interest. Because diffusion was neglected, all chains in an ensemble starting at the same location followed the same streamline. The velocity gradient tensor $\boldsymbol{\kappa}$ was computed along the coarse streamline at equal intervals in time, which required interpolation of the finite element flow solution. Each quadrilateral element was subdivided into eight triangles and the velocity $\mathbf{v}_n$ and the velocity gradients $\boldsymbol{\kappa}_n$ were interpolated at location $\mathbf{x}_n$ using piecewise linear shape functions and the continuum flow solution (velocity and velocity gradients) at the nine nodes.

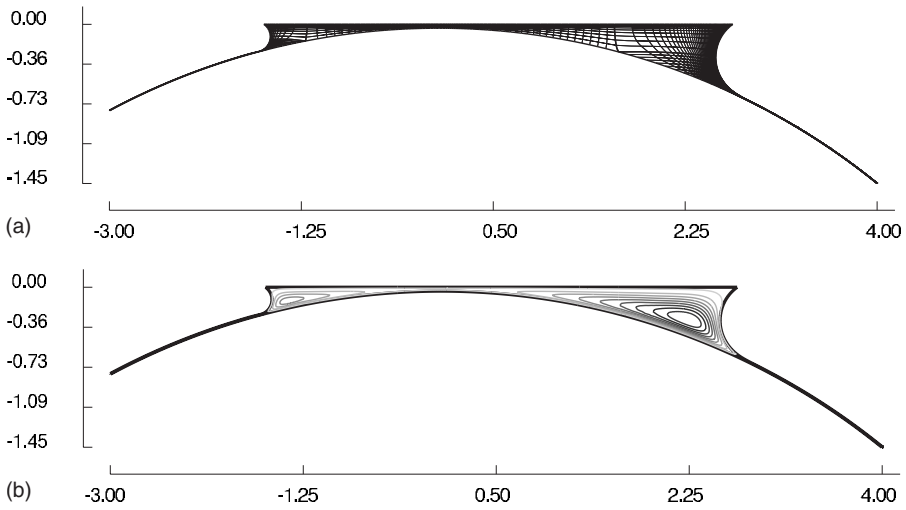

FIG. 2. (a) Finite element mesh solution (2600 elements, 50 844 degrees of freedom) of the roll-knife coating flowcell. The dimensions are in mm. The radius of the roll is $R=6.35$ mm and the gap is $H=35.3$ μm. The capillary number of the flow was Ca=0.0011. The results correspond to the low capillary number experiments E4 and E8 (Duggal and Pasquali, 2004). (b) Streamlines showing the large recirculation below the coverslip.

III. RESULTS AND DISCUSSION

A. Macroscopic flow

Figure 2(a) shows the computed free surface liquid domain at Ca=0.0011 [experiments E4 and E8 in Duggal and Pasquali (2004)]. The number of elements in the mesh is 2600 with ten elements at the minimum gap position ($x=0$). It was found that the flow field and the geometry of the liquid domain (free surfaces) were independent of the discretization of the physical domain. The length of the coating bead was computed to be $l=4.3$ mm.

In a similar but large scale roll-plate setup, Gaskell *et al.* (1998) found that at small flow rates (low capillary numbers) the pressure in the coating bead was entirely subambient with an almost linear gradient typical of meniscus roll coating. We also found that the pressure along the coverslip ($y=0$) in the coating bead, delimited by the contact lines, is subambient with a linear gradient in the middle of the bead ($-0.5\leqslant x\leqslant 0.5$ mm). Because the downstream free surface is less curved as compared to the upstream free surface, the pressure downstream was higher than that upstream causing a backflow which yielded a Couette–Poiseuille flow in the bead (Fig. 3). In the experiments the DNA molecules were observed flowing opposite to the direction of motion of roll just below the coverslip; and lowering the imaging plane into the bead closer to the roll surface revealed DNA moving in the direction of the roll [Duggal and Pasquali (2004)]. Tracking of the molecules next to the coverslip showed that a recirculation existed from the downstream to the upstream free surface. In agreement with experimental observations, the streamlines computed in the flow field show this large recirculation below the coverslip [Fig. 2(b)].

The difference between the computed and measured flow rates was 2.12%. At the minimum gap, the computed velocity agreed well with the lubrication approximation solution (Fig. 3). The average velocity at the two observation planes E4 $y=-3.3$ μm and E8 $y=-21.8$ μm was measured by tracking the center of mass of the DNA molecules as they traversed the field of view. These velocities are also plotted in Fig. 3 for comparison.

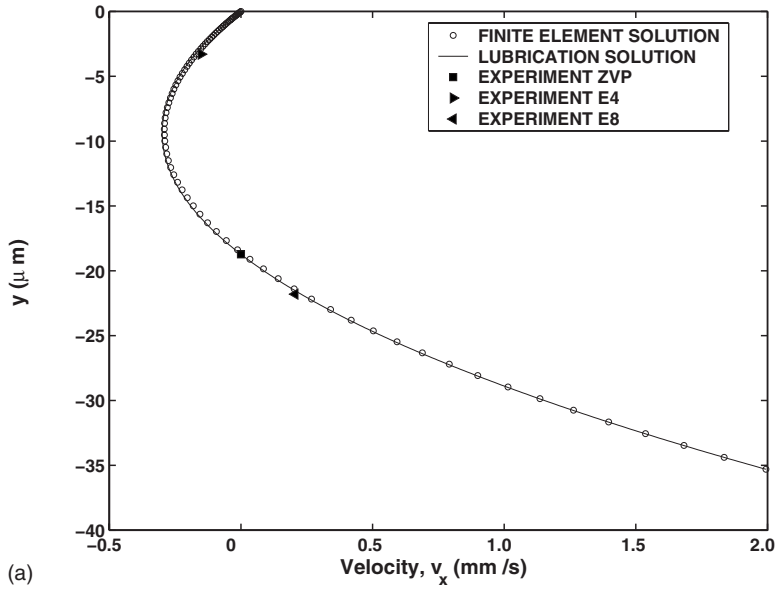

FIG. 3. Comparison of the velocity profile at minimum gap ($x=0$) computed by finite elements ○ and that computed by lubrication approximation (solid line). The experimentally measured velocities at the various image planes (zero velocity plane ZVP, E4, and E8) are also plotted.

B. DNA conformation

The DNA molecules moving along the two experimentally investigated image planes (E4 and E8) at the minimum gap ($x=0$) were trapped in a recirculation. The local Weissenberg Wi numbers at E4 and E8 were 176 and 361, respectively [Duggal and Pasquali (2004)]. The average Weissenberg number $\mathrm{Wi}^e \equiv \lambda v_s / H$ for the flow is 240. Note that Wi is much higher than Wi^e in some regions of the flow.

Before comparing the simulations with experiments it is important to understand the effect of flow on the molecular stretch as the chains traverse along the streamline in the large recirculation. It was found that the initial configuration of the ensemble at the starting location ($x=0$) along the streamline in the recirculation had no effect on the chain conformation at the end of one complete circulation (see supplementary material in EPAPS document E-JORHD2-52-007806). Because diffusion across streamlines was neglected, chains that are part of the recirculation continue to cycle around in the flow; the computed ensemble averaged configuration was independent of the number of cycles (see supplementary material in EPAPS document E-JORHD2-52-007806). Figures 4(c) and 4(d)show the ensemble averaged fractional molecular extension along the x and y axis for seven bead chains along a streamline through $x=0$, $y=-7$ μm [Fig. 4(a)]. The ensemble starts with ~50% extension along x (extensions after completion of one recirculation are shown) at position A. Because this is above the zero-velocity plane, the chains flow opposite the roll ($x<0$) and are aligned with the x axis [Fig. 4(b)]. The chains maintain their extension along x as they approach the free-surface and the contact line at B [Fig. 4(b)]. As they move along the free surface (C), the chains rotate [Fig. 4(b)] and the extension along y increases. The molecules almost reach full extension along x as they cross D, the stagnation point at the free surface. The principal axis of extension at D is normal to the free surface, and the molecules reach high extensions along x as they pass through D onward to E. This stretched configuration is maintained as the chains cross E,

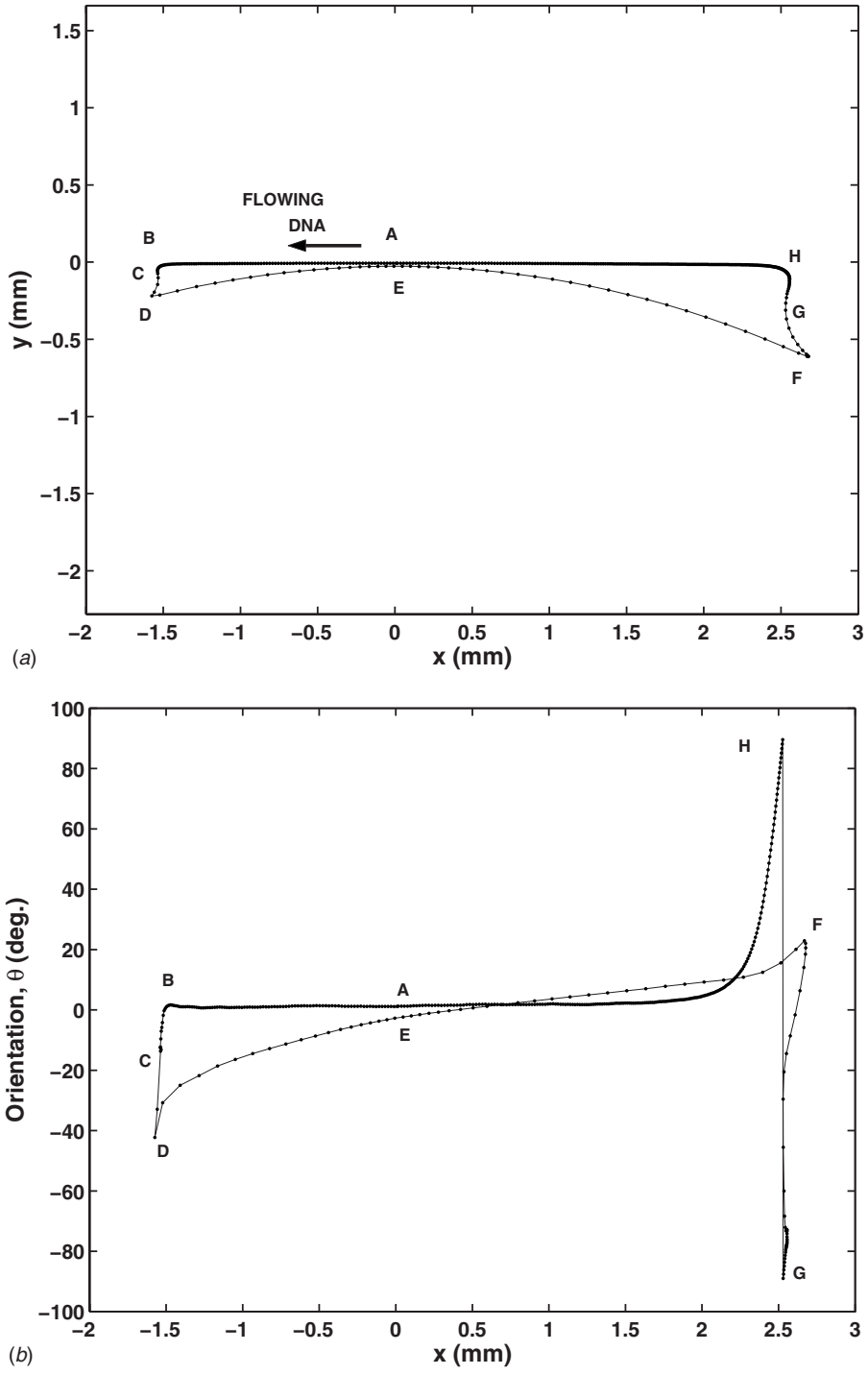

FIG. 4. Extension map of $N=7$ bead-spring chain in the two-dimensional flow. (a) Streamline through $x=0$, $y=-7$ μm in the recirculation region. (b) Ensemble averaged orientation of the chains as a function of position. Zero is along the x axis or the flow direction. (c) Mean fractional extension along x direction as a function of position. (d) Mean fractional extension along y direction as a function of position. A–H are position markers for easier reading. The results are for an ensemble of 100 chains and the error bars are not shown for clarity.

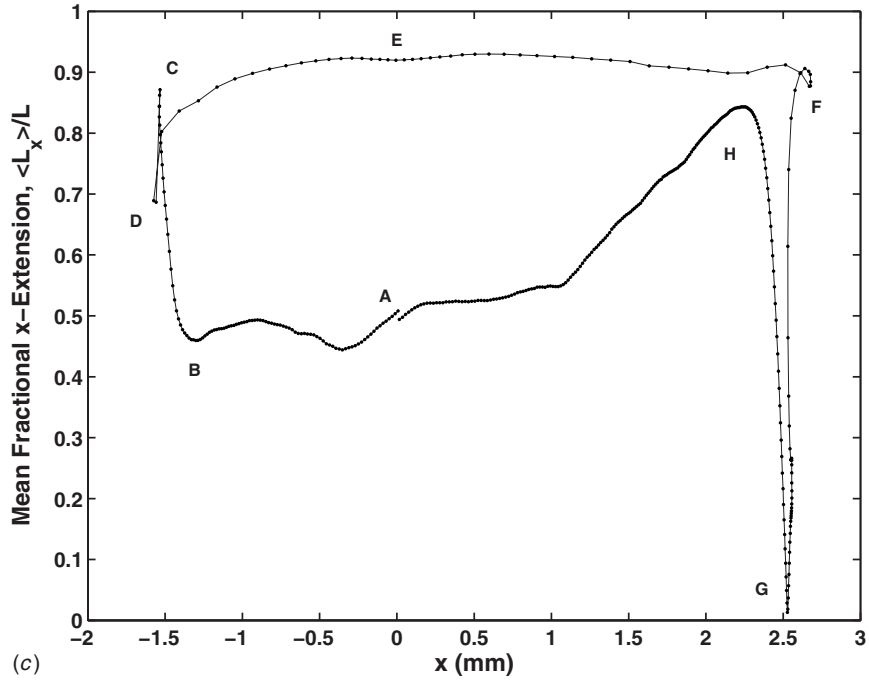

(*c*)

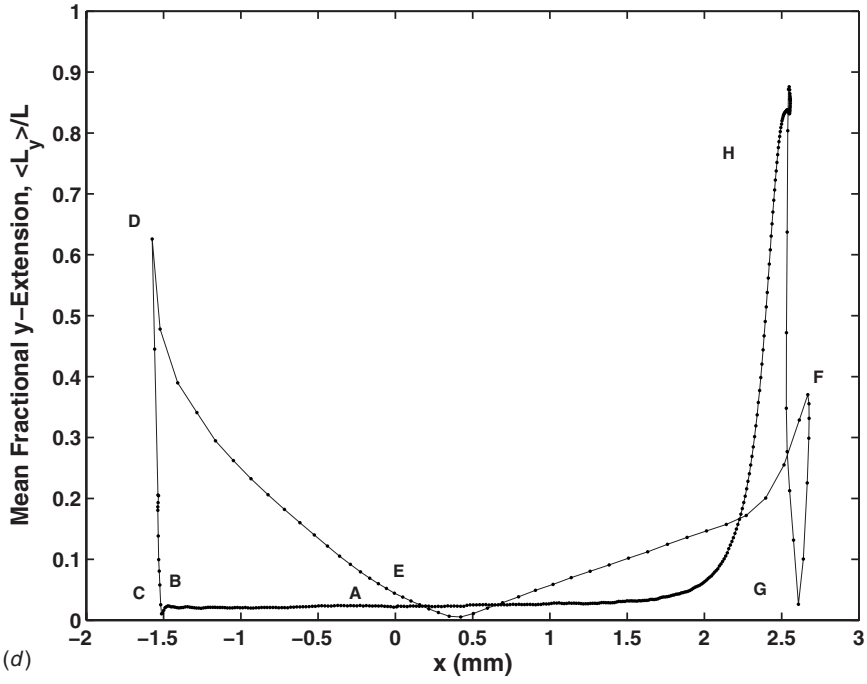

(*d*)

FIG. 4. (*Continued*).

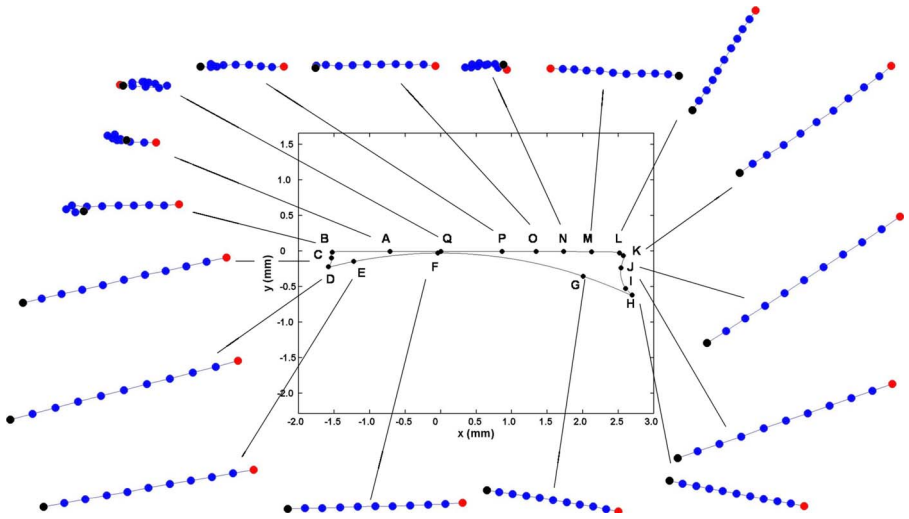

FIG. 5. Images of a single chain of 11 beads moving along a streamline through $x=0$, $y=-3.3$ μm. Tracking the end beads shows the change in the orientation of the molecule as the chain flows.

the minimum gap position $x=0$, because the time taken by the molecule to go from D to E is smaller than the relaxation time. At the stagnation point F on the downstream free surface, the principal axis of compression is normal to the free surface, while the principal axis of extension is along the free-surface; hence, the chains contract along x and extend along y (from G to H). The extended molecules rotate to the x axis as they pass near the contact line at H [Fig. 4(b)]. This extension mapping is qualitatively similar on all streamlines in the recirculation region that cross the minimum gap; see Fig. 5 for a typical trajectory with 11-bead chains along E4.

After extrapolating to $N\rightarrow 250$, the mean fractional extension along the x direction of 1000 chains at E4 was 0.54 ± 0.03 and that at E8 was 0.93 ± 0.01; these values were substantially higher than the measured values (x extension 0.33 ± 0.13 at E4 and 0.37 ± 0.17 at E8). The computed and measured fractional extensions show that molecular conformation is position dependent at the minimum gap; this is expected because each plane experiences a different shear rate. However, in pure homogeneous shear flows, the mean fractional extension is expected to asymptote to 0.5 [Hur *et al.* (2000); Smith *et al.* (1999)]. Although experimental information was obtained at only two planes in this specific flow state, the measured extension was below $\sim$50% at various locations above and below the zero-velocity plane in the minimum gap in all experiments at low capillary number. All the flow states (corresponding to E1–E8) were very similar, and displayed a large recirculation under the coverslip despite minor differences in gap and capillary number [Duggal and Pasquali (2004)]. Therefore, it is reasonable to infer that the DNA extension at the minimum gap should remain below $\sim$50% throughout the gap at the flow conditions of experiments E4 and E8. Simulations were performed at this flow conditions at different y planes at $x=0$. Figure 6 shows the computed mean fractional extension as a function of position at the minimum gap. An abrupt change in the extension computed by Brownian dynamics was found at the zero-velocity plane. The chains reached about 50% extension in the backflow region (molecules moving against the roll); below the zero-velocity plane, i.e., in the forward-flow region, the chains stretched nearly completely. Such strong stretch was accumulated in the strong extensional flow at the upstream free surface (with the principal axis of extension nearly aligned along the roll) and

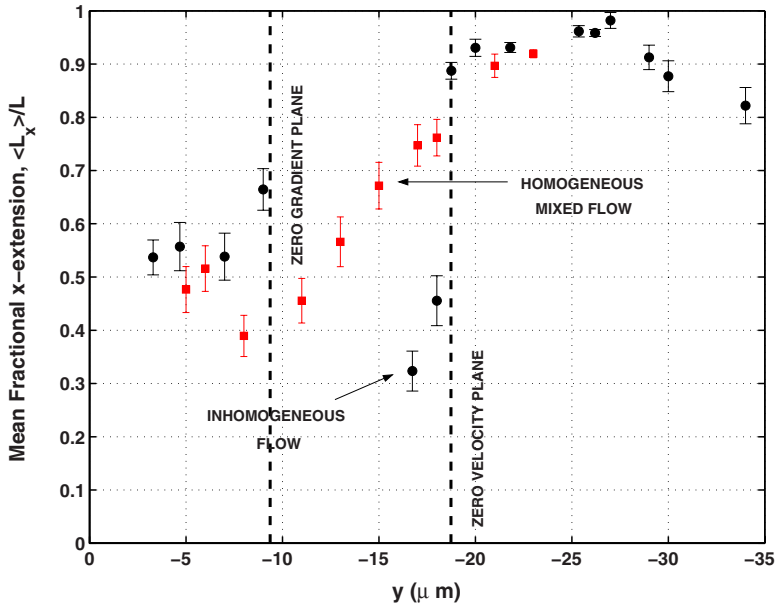

FIG. 6. SFG predictions for molecular extension at different positions in the gap. Extrapolated mean fractional x extension $\langle x\rangle/L$ as a function of position y in the gap for mixed homogeneous flow (red, □) and for inhomogeneous flow in the recirculation (black, ●). The extensions were extrapolated in the limit $N_k \to 250$.

propagated to the minimum gap region because the chains traversed at high speed the region of the bead between the upstream free surface and the minimum gap and did not have time to relax.

We investigated four reasons that could cause this disagreement between the measurements and the simulations in the forward-flow region (below the zero velocity plane, near the roll)—mesh discretization, mixed nature of flow at the minimum gap, wall hydrodynamics, and interference of chain and flow lengthscales. The effect of the mesh refinement was assessed by halving the mesh size and retracing the same streamline. The computed extension agreed well everywhere (including at $x=0$, the region of interest) except for minor differences near the upstream and downstream free surfaces, where the streamline curvature is highest. Because the measured location of the contact lines and flowrate agreed with the finite element results, the discrepancies between measured and simulated DNA conformations cannot be attributed to insufficient accuracy in the flow calculations.

The two-dimensional roll-knife coating flow is a mixed flow, i.e., the flow is a combination of rotation and extension. In homogeneous mixed flows Hur *et al.* (2002) and Babcock *et al.* (2003) found that when the strain rate exceeded the vorticity even slightly (extension dominated flows), the polymer molecules deformed to almost fully stretched states; when the vorticity exceeded the strain rate (rotation dominated flows), the molecules deformed in a periodic motion with an average extension lower than that observed in simple shear flows. The flow-type (extension or rotation dominated) at $x=0$ was determined by computing both the frame-invariant index of Astarita (1979) and Schunk and Scriven (1990), and the frame-dependent measure of Babcock *et al.* (2003). Both these approaches classify the flow below the zero velocity plane ($y<-9$ μm) as slightly extension-dominated; according to the criterion of Schunk and Scriven (1990), the flow above the zero velocity plane was slightly extension-dominated, whereas according to the

measure of Babcock *et al.* (2003) the flow was slightly rotation-dominated [see Duggal, (2006) for details]. The index of Babcock *et al.* (2003) is not frame invariant because it depends explicitly on the vorticity; thus, if the frame of reference is placed on the roll, the value of the flow index changes. Conversely, the flow index of Schunk and Scriven (1990) is frame invariant because it involves only relative rotation rates. In steady, homogeneous flows the two classification approaches are equivalent but in steady, inhomogeneous flows the Schunk and Scriven (1990) approach is more appropriate.

Homogeneous flows with $\boldsymbol{\kappa}$ obtained at different depths at $x=0$ were applied to the ensemble of chains. It was found (Fig. 6) that the slight extension below the zero velocity gradient plane ($y<-9$ μm) was enough to cause the molecules to extend more than that in pure shear (50% molecular extension). The computed extension (along x) grows monotonically at $y<-9$ μm, unlike the abrupt discontinuity computed in the recirculation simulations (Fig. 6). This reinforces that the strain history is important in determining the polymer configuration in inhomogeneous flows.

Another important consideration in microscale flows of polymer molecules is the effect of hydrodynamic forces near solid boundaries. Such forces cause DNA to migrate away from the walls and toward the center of microfluidic channels [Fang *et al.* (2005); Jendrejack *et al.* (2003, 2004)] and depress molecular stretch in a region comparable to the stretched end-to-end distance of the DNA [Fang *et al.* (2005); Woo *et al.* (2004)]. Although we neglected wall hydrodynamic effects and modifications of the entropic spring force due to wall confinement [Woo *et al.* (2004)] in our Brownian dynamics simulations, in the experiments the DNA molecules were observed near walls (3.3 μm away from the coverslip in experiment E4 and 13.5 μm away from the roll in experiment E8); therefore, wall effects may have also contributed to the discrepancy between simulations and experiments.

The fluid velocity about a point in the fluid domain $\mathbf{x}$ can be expanded in Taylor series as

$$\mathbf{v}(\mathbf{x}+\mathbf{dx}) \approx \mathbf{v}(\mathbf{x}) + \mathbf{dx}\cdot\boldsymbol{\nabla}\mathbf{v} + \frac{1}{2}\mathbf{dxdx}:\boldsymbol{\nabla}\boldsymbol{\nabla}\mathbf{v} + O(|\mathbf{dx}|^3). \tag{8}$$

In nearly all Brownian dynamics simulations (including this study), the velocity of the fluid at a bead i located at position $\mathbf{x_i}$ is expressed in terms of the velocity of the fluid at the center of mass $\mathbf{x}$ of the chain by using the linear approximation

$$\mathbf{v}(\mathbf{x}_i) \approx \mathbf{v}(\mathbf{x}) + \mathbf{r}_i\cdot\boldsymbol{\nabla}\mathbf{v}, \tag{9}$$

where $\mathbf{r}_i \equiv \mathbf{x}_i - \mathbf{x}$ is the distance of the bead from the center of mass. Comparing Eqs. (8) and (9) shows that the simple linear velocity assumption holds when

$$\mathbf{r}_i\mathbf{r}_i:\boldsymbol{\nabla}\boldsymbol{\nabla}\mathbf{v} \ll \mathbf{r}_i\cdot\boldsymbol{\nabla}\mathbf{v}. \tag{10}$$

The term on the right is of order ε, that on the left of order ε^2, where $\varepsilon \equiv \ell/h$ is the ratio of a microscopic lengthscale ℓ related to the polymer and a macroscopic lengthscale h related to the flow; hence, the linear velocity assumption in Eq. (9) is valid only where $\varepsilon \ll 1$. In the absence of flow, λ-DNA has a characteristic length of about 0.7 μm (radius of gyration), which is about 2% of the characteristic length scale of the flow (minimum gap $h \approx H = 35$ μm). By this metric, $\varepsilon \approx 0.02 \ll 1$. However, in a strong flow, the microscopic lengthscale is better represented by half of the contour length, i.e., $\ell \approx 11$ μm, in case of stained λ-DNA; in the region of the flow near the stagnation point on the upstream free surface (e.g., location D in Fig. 5), the characteristic length scale is comparable to the upstream film thickness, i.e., $h \approx 10$ μm. Clearly, $\varepsilon \approx 1$, and the approximation of linear velocity on the molecule lengthscale fails.

To test the effect of the (poor) linear velocity approximation, single seven-bead chains were simulated and tracked along the streamline corresponding to E4 (see Fig. 5 for a typical trajectory). In the minimum gap region, the chains are coiled or stretched along the streamwise direction, where the velocity changes slowly; the linear velocity assumption works well, and the chains lie inside the fluid domain. Conversely, near the stagnation points on the upstream and downstream free surfaces, the chains approach full extension and the velocity field changes abruptly over short [a few microns (μm)] distances; in these regions of the flow (Fig. 7), parts of the chains cross the free surface, which is unphysical, and shows that the assumption of linear velocity across the molecule is not valid.

Chains coming from the upstream free surface move quickly along the streamlines, because the velocity is high in that region. Thus, they do not have sufficient time to "forget" their stretch before reaching the minimum gap location (point of observation); this is the likely cause of the discrepancy between experimental observations and model predictions at the minimum gap below the zero velocity plane.

On the other hand, chains move slowly in the recirculating region from the downstream free surface to the minimum gap. These chains spend several relaxation times in the shear flow in the slowly converging region downstream of the minimum gap and have enough time to "recover" from errors introduced in the simulations. In fact, the measured extension above the zero velocity plane agrees better with the simulations.

It is interesting to discuss the findings of this study in relevance to common microscale operations such as coating and ink-jet printing of polymer solutions. Synthetic polymer molecules that are commonly used as thickeners in coating and ink-jet fluids—e.g., polyethylene oxide (PEO) and PS—have contour length (and radius of gyration) similar to that of DNA molecules used in this study; 5 Mg/mol PEO has contour length $\sim$48 μm and 10 Mg/mol PS has contour length $\sim$26 μm. In ink-jet printing, nozzle and droplet sizes are in the 10 μm and 10 pL range, respectively. In the preparation of DNA microarrays, droplets are in the pL range ($\approx$10 μm) and spot sizes 15–300 μm [Blossey and Bosio (2002); Cooley *et al.* (2001)]. In liquid film coating, gaps below $\approx$100 μm and wet film thickness of few μm to $\sim$ tens of μm are commonplace [Gutoff *et al.* (1995)]. Shear and extension rates (usually above 10^3 s^{-1} and often in excess of 10^4 s^{-1}) are certainly strong enough to stretch long polymers (relaxation times in the tens to hundreds of (milliseconds) to a relevant fraction of their contour length. Therefore, it is possible that in many coating and jetting flows, there is interference of lengthscales between process and polymer. In the present study, λ-DNA of contour length 22 μm were investigated in a roll-knife coating flow with gap $\sim$35 μm, and the film thickness was $\sim$10 μm. The ratio of polymer to flow length scale ($L/2h$) ranges from 0.02 to 1.1. Previous state of the art studies on coating flows of polymer solutions [Dontula (1999); Lee (2001)] also have similar ratio of the lengthscales, i.e., the ratio of polymer to flow length scale is O(1). Dontula (1999) studied various coating flows—roll, slide, and slot coating—of PEO with molecular weight 4–7 Mg/mol (estimated contour length $\sim$38–66 μm). In roll coating flow experiments [Chap. 5, p. 127 in Dontula (1999)] the gap used was 100 μm and the corresponding estimated film thickness close to 50 μm; the ratio of polymer to flow length scale is about 0.66. In slide coating flow experiments [Chap. 5, p. 132 in Dontula (1999)] the film thickness was about 40 μm and the ratio of polymer to flow length scale is about 0.58. In slot coating flow experiments [Chap. 5, p. 149 in Dontula (1999)] the film thickness was about 60 μm and the ratio of polymer to flow length scale is about 0.31. Lee (2001) studied free-surface displacement flows (Hele-shaw and slot coating flows) of solutions of PS with molecular weight 20 Mg/mol (estimated contour length $\sim$52 μm). In eccentric roll coating flow experiments [Chap. 2, p. 24 in Lee (2001)] the

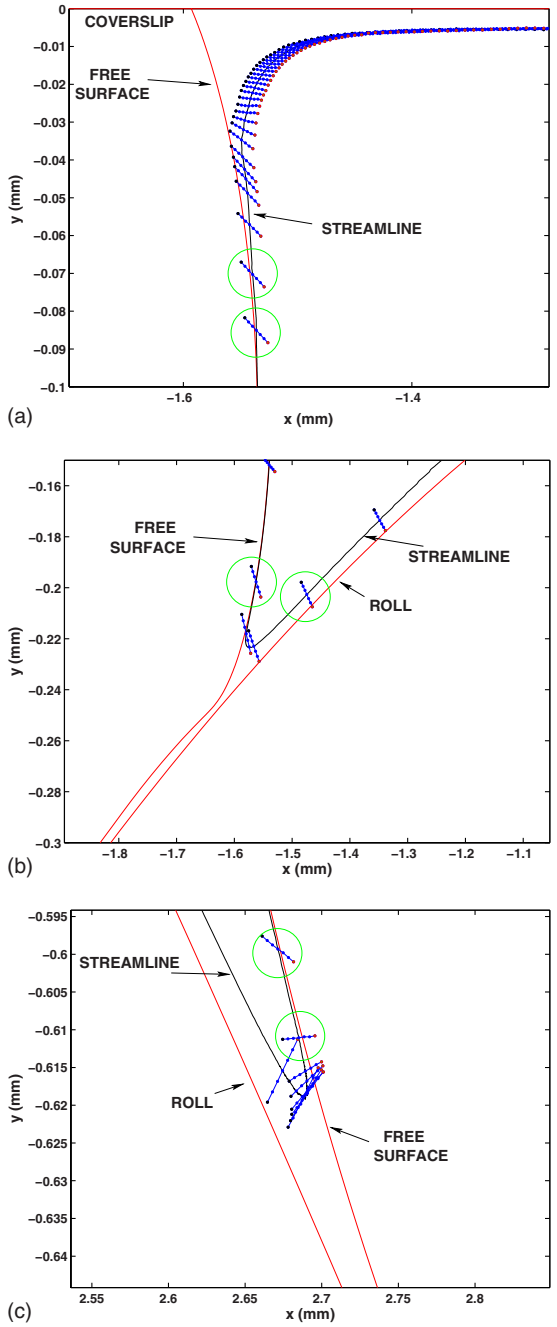

FIG. 7. Snapshots of seven bead chain, traversing along streamline corresponding to E4 ($x=0$ and $y=-3.3$ μm), crossing the liquid domain. (a) Near the upstream free surface. (b) Near the stagnation point at the upstream free surface. (c) Near the stagnation point at the downstream free surface. The liquid domain boundaries—coverslip, roll and the free surfaces—and the streamline are plotted. The center of mass of the chain moves along the streamline. A few chains that cross the liquid domain are encircled in each plot.

gap used was from 200 to 1000 μm [Chap. 3, p. 36 in Lee (2001)] and the corresponding film thickness would be close to 100–500 μm or less [p. 62, Fig. 3.40 gap b=60 μm in Lee (2001)]. Therefore, the ratio of polymer to flow length scale ranged from about 0.05 to 0.26 (0.43 for Fig. 3). Solutions of poly-iso-butylene with molecular weight 4–6 Mg/mol (estimated contour length from 23 to 35 μm) were also investigated. The ratio of polymer to flow length scale ranged from about 0.02 to 0.18. Therefore, interference between molecular and flow lengthscales has been reported before in coating flows of common synthetic polymer solutions—although no specific reference was made to the overlap of these two lengthscales. Thus, the assumptions of separation of lengthscales implicit in models based on continuum constitutive equations or conformation tensor models used in recent analysis of viscoelastic coating and ink-jet flows [Bajaj *et al.* (2006); Bhat (2007); Dimakopoulos and Tsamopoulos (2004); Lee *et al.* (2002); Pasquali and Scriven (2002)] may have to be carefully revisited.

IV. CONCLUSIONS

The configuration of DNA molecules in a complex free surface flow has been computed by a multiscale method and compared to previous measurements of ultradilute solutions of DNA in sugar and water. The measured and computed macroscopic flow features agreed well. Brownian dynamics simulations using SFG that have been shown to predict qualitatively homogeneous flows of dilute polymer solutions failed to predict DNA stretch observed in the experiments. The commonly used assumption that velocity is linear across the dimensions of a polymer (DNA) molecule fails in a small-gap coating flow because the DNA molecules stretch to a contour length that is comparable to the characteristic dimension of the flow. Therefore, a new framework is needed to handle complex coating flows that are inhomogeneous on the length scale of a polymer molecule. The focus in the past has been in improving constitutive relations for homogeneous flows; however, for relevant and realistic flows such as the one used in the present study, focusing only on developing better constitutive models does not guarantee successful quantitative predictions. Future models and simulations of such microscale flows should include a more complete representation of the velocity field at each bead. Although tracking each bead in the flow (rather than the center of mass) is algorithmically trivial, it will largely increase computational costs, because it requires interpolating the velocity at each bead of each chain at each time step (rather than precomputing the velocity and velocity gradient at prefixed points along a streamline). Therefore, more clever algorithms are needed for tracking (or estimating) accurately the velocity of the polymer beads in regions of the flow where the linear velocity approximation fails.

The multiscale approach used here should be improved to include a more accurate representation of the flow field in the Brownian dynamics simulation. Such improved approach can complement single molecule DNA experiments to understand polymer dynamics in other complex microscale flows of ultradilute solutions and can be used to test, validate, and extend molecular models for dilute polymer solutions, on the way towards fully coupled simulations where the deformation of the microstructure also affects the flow field.

ACKNOWLEDGMENTS

The authors would like to thank X. Xie, D. Arora, G. Zevallos and O. C. Matutti. This work was supported by the National Science Foundation through Grant No. CTS-CAREER 0134389, by the NSF Center for Biological and Environmental Nanotechnology (EEC-0118007), and through a grant from the Australian Research Council, under

the Discovery-Projects program. Computational resources were provided by the Rice Terascale Cluster funded by NSF under Grant No. EIA-0216467, Intel, and HP.

References

Astarita, G., "Objective and generally applicable criteria for flow classification," J. Non-Newtonian Fluid Mech. **6**, 69–76 (1979).

Babcock, H. P., D. E. Smith, J. S. Hur, E. S. G. Shaqfeh, and S. Chu, "Relating the microscopic and macroscopic response of a polymeric fluid in a shearing flow," Phys. Rev. Lett. **85**, 2018–2021 (2000).

Babcock, H. P., R. E. Teixeira, J. S. Hur, E. S. G. Shaqfeh, and S. Chu, "Visualization of molecular fluctuations near the critical point of the coil-stretch transition in polymer elongation," Macromolecules **36**, 4544–4548 (2003).

Bajaj, M., P. P. Bhat, J. R. Prakash, and M. Pasquali, "Multiscale simulation of viscoelastic free surface flows," J. Fluid Mech. **140**, 87–107 (2006).

Barrat, J.-L., and J.-F. Joanny, "Theory of polyelectrolyte solutions," Adv. Chem. Phys. **94**, 1–66 (1996).

Bhat, P. P., "The dynamics of filaments of complex liquids analyzed by continuum and mixed continuum-stochastic methods," Ph.D. thesis, Rice University, Houston, TX, 2007, available from UMI, Ann Arbor, MI, 3256661.

Bird, R. A., C. F. Curtiss, R. C. Armstrong, and O. Hassager, *Dynamics of Polymeric Liquids*, 2nd ed. Vol. 2 (Wiley, New York, 1987).

Blossey, R., and A. Bosio, "Contact line deposits on cdna microarrays: A 'twin-spot effect'," Langmuir **18**, 2952–2954 (2002).

Carvalho, M. S., "Roll coating flows in rigid and deformable gaps," Ph.D. thesis, University of Minnesota, Minneapolis, MN, 1996, available from UMI, Ann Arbor, MI, Order No. 9621887.

Carvalho, M. S., and H. S. Kheshgi, "Low-flow limit in slot coating: Theory and experiments," AIChE J. **46**, 1907–1917 (2000).

Chopra, M., L. Li, H. Hu, M. A. Burns, and R. G. Larson, "Dna molecular configurations in an evaporating droplet near a glass surface," J. Rheol. **47**, 1111–1132 (2003).

Christodoulou, K. N., "Computational physics of slide coating flow," Ph.D. thesis, University of Minnesota, Minneapolis, MN, 1990, available from UMI, Ann Arbor, MI, Order No. 9021329.

Christodoulou, K. N., S. F. Kistler, and P. R. Schunk, "Advances in computational methods for free-surface flows," in *Liquid Film Coating. Scientific Principles and Their Technological Implications*, edited by S. F. Kistler and P. M. Schweizer (Chapman & Hall, London, 1997), pp. 297–366.

Cooley, P., D. Wallace, and B. Antohe, "Applications of ink-jet printing technology to biomems and microfluidic systems," in Proceedings SPIE Conference on Microfluidics and BioMEMS, San Fransisco, CA, 2001.

de Gennes, P. G., "Polymer physics—Molecular individualism," Science **276**, 1999 (1997).

de Santos, J. M., "Two-phase cocurrent downflow through constricted passages," Ph.D. thesis, University of Minnesota, Minneapolis, MN, 1991, available from UMI, Ann Arbor, MI, Order No. 9119386.

Dimakopoulos, Y., and J. Tsamopoulos, "On the gas-penetration in straight tubes completely filled with a viscoelastic fluid," J. Non-Newtonian Fluid Mech. **117**, 117–139 (2004).

Doi, M., and S. F. Edwards, *The Theory of Polymer Dynamics*, 1st ed. (Oxford University Press, Oxford, 1986).

Dontula, P., "Polymer solutions in coating flows," Ph.D. thesis, University of Minnesota, Minneapolis, MN, 1999, available from UMI, Ann Arbor, MI, Order No. 9937847.

Duggal, R., "Interplay of micro-scale flow and fluid micro/nanostructure: Solutions of DNA and suspensions of single walled carbon nanotubes," Ph.D. thesis, Rice University, TX, 2006, available from UMI, Ann Arbor, MI, order No. 3216698.

Duggal, R., and M. Pasquali, "Visualization of individual dna molecules in a small-scale coating flow," J. Rheol. **48**, 745–764 (2004).

Fang, L., H. Hu, and R. G. Larson, "DNA configurations and concentration in shearing flow near a glas surface in a microchannel," J. Rheol. **49**, 127–138 (2005).

Flory, P. J., *Principles of Polymer Chemistry*, 1st ed. (Cornell University Press, Ithaca, 1953).

Gallez, X., P. Halin, G. Lielens, R. Keunings, and V. Legat, "The adaptive Lagrangian particle method for macroscopic and micro-macro computations of time-dependent viscoelastic flows," Comput. Methods Appl. Mech. Eng. **180**, 345–364 (1999).

Gaskell, P. H., G. E. Innes, and M. D. Savage, "An experimental investigation of meniscus roll coating," J. Fluid Mech. **355**, 17–44 (1998).

Gutoff, E. B., E. D. Cohen, and G. I. Kheboin, *Coating and Drying Defects: Troubleshooting Operating Problems*, (Wiley, New York, 1995).

Harrison, G. M., J. Remmelgas, and L. G. Leal, "The dynamics of ultradilute polymer solutions in transient flow: Comparison of dumbbell-based theory and experiment," J. Rheol. **42**, 1039–1058 (1998).

Hulsen, M. A., A. P. G. van Heel, and B. H. A. A. van den Brule, "Simulation of viscoelastic flow using Brownian configuration fields," J. Non-Newtonian Fluid Mech. **70**, 79–101 (1997).

Hur, J. S., E. S. G. Shaqfeh, H. P. Babcock, and S. Chu, "Dynamics and configurational fluctuations of single dna molecules in linear mixed flows," Phys. Rev. E **66**, 011915 (2002).

Hur, J. S., E. S. G. Shaqfeh, H. P. Babcock, D. E. Smith, and S. Chu, "Dynamics of dilute and semidilute DNA solutions in the start-up of shear flow," J. Rheol. **45**, 421–450 (2001).

Hur, J. S., E. S. G. Shaqfeh, and R. G. Larson, "Brownian dynamics simulations of single DNA molecules in shear flow," J. Rheol. **44**, 713–742 (2000).

Jendrejack, R. M., J. J. de Pablo, and M. D. Graham, "Stochastic simulations of DNA in flow: Dynamics and the effects of hydrodynamic interaction," J. Chem. Phys. **116**, 7752–7759 (2002).

Jendrejack, R. M., E. T. Dimalanta, D. C. Schwartz, M. D. Graham, and J. J. de Pablo, "DNA dynamics in a microchannel," Phys. Rev. Lett. **91**, 038102 (2003).

Jendrejack, R. M., D. C. Schwartz, J. J. de Pablo, and M. D. Graham, "Shear-induced migration in flowing polymer solutions: Simulation of long-chain DNA dynamics in microchannels," J. Chem. Phys. **120**, 2513–2529 (2004).

Larson, R. G., *The Structure and Rheology of Complex Fluids*, 1st ed. (Oxford University Press, New York, 1999).

Larson, R. G., H. Hu, D. E. Smith, and S. Chu, "Brownian dynamics simulations of a DNA molecule in an extensional flow field," J. Rheol. **43**, 267–304 (1999).

Laso, M., and H. Öttinger, "Calculation of viscoelastic flow using moleculat models: the CONNFFESSIT approach," J. Non-Newtonian Fluid Mech. **47**, 1–20 (1993).

Lee, A. G., "Viscoelastic effects on free surface displacement flows: A computational and experimental study," Ph.D. thesis, Stanford University, Palo Alto, CA, 2001, available from UMI, Ann Arbor, MI, Order No. 3038115.

Lee, A. G., E. S. G. Shaqfeh, and B. Khomami, "A study of viscoelastic free surface flows by the finite element method: Hele-Shaw and slot coating flows," J. Non-Newtonian Fluid Mech. **108**, 327–362 (2002).

Marano, R. S., J. M. Smolinski, C. W. Manke, E. Gulari, and R. L. Messick, "Polymer additives as mist suppressants in metal cutting fluids," Lubr. Eng. **53**, 25–36 (1997).

Marko, J. F., and E. D. Siggia, "Stretching DNA," Macromolecules **28**, 8759–8770 (1995).

Öttinger, H. C., *Stochastic Processes in Polymeric Fluids*, 1st ed. (Springer, Berlin, 1996).

Papanastasiou, T. C., N. Malamantaris, and K. Ellwood, "A new outflow boundary condition," Int. J. Numer. Methods Fluids **14**, 587–608 (1992).

Pasquali, M., "Polymer molecules in free surface coating flows," Ph.D. thesis, University of Minnesota, Minneapolis, MN, 2000, available from UMI, Ann Arbor, MI, Order No. 9963019.

Pasquali, M., and L. E. Scriven, "Free surface flows of polymer solutions with models based on the conformation tensor," J. Non-Newtonian Fluid Mech. **108**, 363–409 (2002).

Perkins, T. T., D. E. Smith, and S. Chu, "Single polymer dynamics in an elongational flow," Science **276**, 2016–2021 (1997).

Perkins, T. T., D. E. Smith, R. G. Larson, and S. Chu, "Stretching of a single tethered polymer in a uniform flow," Science **268**, 83–87 (1995).

Prabhakar, R., and J. R. Prakash, "Multiplicative separation of the influences of excluded volume, hydrodynamic interactions and finite extensibility on the rheological properties of dilute polymer solutions," J.

Non-Newtonian Fluid Mech. **116**, 163–182 (2004).

Prabhakar, R., J. R. Prakash, and T. Sridhar, "A successive fine-graining scheme for predicting the rheological properties of dilute polymer solutions," J. Rheol. **48**, 1251–1278 (2004).

Rouse, P. E., "A theory of the linear viscoelastic properties of dilute solutions of coiling polymers," J. Chem. Phys. **21**, 1272–1280 (1953).

Schunk, P. R., and L. E. Scriven, "Constitutive equation for modeling mixed extension and shear in polymer solution processing," J. Rheol. **34**, 1085–1119 (1990).

See EPAPS Document No. E-JORHD2-52-007806 for DNA modeling using Successive Fine Graining. For more information on EPAPS, see http://www.aip.org/pubservs/epaps.html.

Shaqfeh, E. S. G., "The dynamics of single-molecule DNA in flow," J. Non-Newtonian Fluid Mech. **130**, 1 (2005).

Smith, D. E., H. P. Babcock, and S. Chu, "Single-polymer dynamics in steady shear flow," Science **283**, 1724–1727 (1999).

Smith, D. E., and S. Chu, "Response of flexible polymers to a sudden elongational flow," Science **281**, 1335–1340 (1998).

Sunthar, P., D. A. Nguyen, R. Dubbelboer, J. R. Prakash, and T. Sridhar, "Measurement and prediction of the elongational stress growth in a dilute solution of dna molecules," Macromolecules **38**, 10200–10209 (2005).

Sunthar, P., and J. R. Prakash, "Parameter-free prediction of dna conformations in elongational flow by successive fine graining," Macromolecules **38**, 617–640 (2005).

Tullo, A. H., "Paints and coatings: Cover story," Chem. Eng. News **82**, 25–31 (2004).

Woo, N. J., E. S. G. Shaqfeh, and B. Khomami, "The effect of confinement on dynamics and rheology of dilute deoxyribose nucleic acid solutions. II. Effective rheology and single chain dynamics," J. Rheol. **48**, 299–318 (2004).

Zimm, B. H., "Dynamics of polymer molecules in dilute solutions: Viscoelasticity, flow birefringence, and dielectric loss," J. Chem. Phys. **24**, 269–278 (1956).